International Journal of Applied Engineering Research ISSN 0973-4562 Volume 12, Number 14 (2017) pp. 4663-4674

Numerical Investigation of a Liquid-Gas Ejector in Marine Ships

Mohammed Esmail Alshebani [#1], Khaled Alawadhi [#2], Abdulwahab A. Alnaqi[*2] and Alaa Ahmed Saker[#1]

[#1] *Water resources department, Higher Institute of Energy, The Public Authority for Applied Education and Training, Kuwait.*
[#2] *Department of Automotive and Marine Engineering Technology, College of Technological Studies, The Public Authority for Applied Education and Training, Kuwait.*

*(*Corresponding author)*

Abstract
The purpose of the current study is performance evaluation of a gas-liquid jet ejector under various conditions numerically. A commercial code ANSYS-CFX has been adopted to solve the computational model. To solve velocity fields of air and water separately mixture model was implemented for the current study. For accurate turbulent boundary layer prediction in the nozzle and mixing flow in the mixing chamber, SST turbulence model was opted. Motive air pressure, suction side pressure and S/D_{th} were varied to see their effect on the secondary fluid flow rate and ratio of secondary to primary flow rate. Mover over flow behavior of primary and secondary fluid in the nozzle wake and mixing chamber has been discussed with various applied conditions. It was evaluated that ratio of secondary to primary fluid flow rate increasing with the increase of motive air pressure initially and then becomes constant at some value of motive air pressure. Moreover maximum flow rate of the secondary fluid was achieved at $\frac{S}{D_{th}} = 1$.

NOMENCLATURE

d	diameter $[m]$
E	total energy [J]
$\mathbf{g}$	gravitational acceleration $[m\ s^{-2}]$
h	specific enthalpy $[J]$
k	thermal conductivity $[W.m^{-1}.K^{-1}]$
L	length $[m]$
$\dot{m}$	mass flow rate $[kg\ s^{-1}]$
N	number of nodes
p	pressure $[Pa]$
S	distance of primary fluid nozzle from the mixing chamber $[m]$
T	Temperature $[K]$
$\mathbf{u}$	velocity vector $[m\ s^{-1}]$
u	velocity magnitude $[m\ s^{-1}]$

Greek letters

α	volume fraction
μ	dynamic viscosity $[kg\ m\ s]$
ρ	density $[kg\ m^{-3}]$

Sub and superscripts

dif	diffuser
ent	entry region
k	extended portion
k	kth phase
mix	mixture
mt	mixing tube
n	total number of phases
noz	nozzle
wt	water connection tube

INTRODUCTION

The jet pump is adevice that works on the principle of exchanging the kinetic energy of the primary fluid with the secondary fluid in the cylinder chamber known as mixture chamber. These devices are utilized to pump a fluid (secondary fluid) (gas, liquid, vapour or two-phase) by mean of other fluid know as primary or motive fluid. Jet pump based on the type of primary and secondary fluid could be characterized as gas-gas, gas-liquid, and liquid-liquid jet ejectors. Gas-liquid jet pumps are widely used due to their diversity of assembly choices, artless design, and absence of moving parts[1]. Jet pumps have numerous applications in hydraulic dredging, nuclear reactor cooling, oil well production and emergency drainages in marine ships. Presently in marine ships, fixed jet ejectors haves replaced bilge and fire pumps in dewatering components, pumping bilges and deballasting. Gas-jet pumps have gained significance in the treatment of ballast water. A small amount of ballast water in pumped through as gas liquid ejectors that drive ozone through the ballast water to kill microorganism of ballast water in marine ships[2].

In literature jet ejectors have been studied experimentally[3], [4], numerically [5]–[7], [2], [8] and using both numerical and experimental methods [9], [10]. Nawar et al. [3] studied different factors that affect the performance of jet pumps that include pressure under which primary is being ejected, suction pressure and $\frac{S}{D_{th}}$. Wenbo et al. [4] conducted an experimental study on gas-gas jet ejector to predict stall conditions induced by the back pressure. Glauber et al. [5] used a one dimensional numerical model for jet pumps for its initial design calculations. performance of a jet pump with circumferential nozzles was evaluated using numerical techniques by Lisowskiet al. [6]. Entrainment behavior and performance of the gas-liquid jet pumps has been investigated by Li et al. They have used numerical model for their study and concluded that for a fixed primary and secondary flow pressures secondary fluid flow rate decreases linearly by increasing pressure difference(Δp) across secondary flow entrainment and exhaust pressure. Song et al. [2] investigated numerically the performance of a liquid- gas jet ejector used for shipping blast water treatment. Performance of single and two stage liquid – liquid jet pump has been evaluated and compared using numerical techniques using different flow rates of primary fluid

by Hassan et al. liquid-gas and liquid jet pumps were evaluated for performance using both numerical and experimental methods by Yuan et al. [9]. They studied effects of different operating variables on the efficiency of the pump. Geometrical optimization study have been conducted by Eves et al. [11] and Yapici et al[12].

It could be deducted from above literature survey that numerical studies on the gas-liquid jet ejectors are rare. That is due to complex flow physics due multi-phase flow along with thepresence of pseudo-shock waves in the wake of thenozzle. The existence of such shock waves is associated with anabrupt change of velocity, pressure and density field. Accurate capturing of this kind of flow physics is vital for the accurate performance prediction of jet ejectors that require very fine and good quality mesh. Multiphase flows and requirement of fine mesh make such numerical studies computationally very difficult and expensive. However, in the current study effect of different parameters on the performance of gas-liquid jet ejector have been studied numerically by addressing above mentioned requirements for such studies. A very high-qualityhexahedral mesh was generated using ICEM-CFD with clustering in the region of high flow derivatives. SST turbulence model has been utilized to capture the boundary layer accurately in the nozzle section and highly turbulent and mixing flow in the mixing tube. Effect of the motive fluid pressure, suction pressure and S/D_{th} have been evaluated on the flow rate of the secondary fluid. Moreover, highlight of the study is flow physics in the nozzle wake and mixing tube has been discussed under varying flow conditions.

COMPUTATIONAL MODEL

Governing equations

Computational domain was solved for steady state solution with two phases i.e. Water and air. Both phases form their own velocity filed in the jet pump thus the interaction of one field with the other was solved by employing mixture model. Slip velocities between the two phases on which drag forces between the two phases are highly dependent were computed using Manninen assumptions. Steady state governing equations of continuity, momentum, and energy employed for the current study are given in Eqs (1-3)

Continuity equation

$$\nabla.(\rho_{mix}\mathbf{u}_{mix}) = 0 \tag{1}$$

Here $\mathbf{u}_{mix}$ is the mass average velocity vector of the mixture

$$\mathbf{u}_{mix} = \frac{\sum_{k=1}^{n}\alpha_k\rho_k\mathbf{u}_k}{\rho_{mix}} \tag{2}$$

Mixture density ρ_m could be computed using Eq. 3

$$\rho_{mix} = \sum_{k=1}^{n}\alpha_k\rho_k \tag{3}$$

In the above equations index, "*k*" represent a phase and n is a total number of phases. The current study involves two phases that are liquid (water and Gas (air). α_k represents the volume fraction of phase k.

Momentum equation

Momentum equation given in equation is written by summing up momentum equation for all individual phases.

$$\nabla.(\rho_{mix}\mathbf{u}_{mix}\mathbf{u}_{mix}) = \nabla p + \nabla.[\mu_{mix}(\nabla\mathbf{u}_{mix} + \nabla\mathbf{u}_{mix}^{T})] + \rho_{mix}\mathbf{g} + F + \nabla.\left(\sum_{k=1}^{n}\alpha_k\rho_k\mathbf{u}_{drift,k}\,\mathbf{u}_{drift,k}\right) \tag{4}$$

Here p , μ_{mix}, $\mathbf{g}$ and $\mathbf{u}_{drift,k}$ are pressure, average viscosity of mixture, acceleration due to gravity vector and drift velocity vector of phase k respectively. Average viscosity of the mixture and drift velocity of the phase *k* could be computed using the equations below.

$$\mu_m = \sum_{k=1}^{n}\alpha_k\mu_k \tag{5}$$

$$\mathbf{u}_{drift,k} = \mathbf{u}_k - \mathbf{u}_{mix} \tag{6}$$

Energy Equation

Alike to momentum equation, energy equation for the mixture is obtained by summing up the energy equation of individual phase and is given in the Eq. 7.

$$\nabla.\sum_{k=1}^{n}\left(\alpha_k\mathbf{u}_k(\rho_k E_k + p)\right) = \nabla.\left(k_{eff}\nabla T\right) + S_E \tag{7}$$

In the above equation $k_{eff}$is the effective thermal conductivity that is define by the Eq. 8

$$k_{eff} = \sum_{k=1}^{n}\alpha_k(k_k + k_t) \tag{8}$$

$k_t$is the turbulent thermal conductivity based on the turbulence model. Term $\nabla.\left(k_{eff}\nabla T\right)$ represents the energy transfer due to conduction while term S_E is the volumetric heat source term. The term E_k in the left hand side of the equation is defined in Eq. 9 for compressible phase.

$$E_k = h_k - \frac{p}{\rho_k} + \frac{u_k^2}{2} \tag{9}$$

Here $h_k$is the sensible enthalpy term for phase *k*. For incompressible phase above equation reduces to $E_k = h_k$.

For the numerical closure of the Reynold stress tensor term in the momentum equation, SST Turbulence Model is used. SST $k-\omega$ turbulence model is adopted due to its capability of computing boundary layer accurately. Although standard $k-\epsilon$ model require less computational resources and recommended by Li et al. [7] for similar studies yet SST $k-\omega$ was preferred as standard $k-\epsilon$ model is incapable of resolving the boundary layer accurately. Details of the SST turbulence model could be found in [13].

Geometrical model

Geometrical model of the jet pump used for the study is shown

in the Fig. 1. The main body of jet pump consists of thesuction nozzle, mixing tube/chamber and diffuser. Suction nozzle is supplied with a pipe with inner diameter $d_{st} = 43\ mm$connected with water reservoir. Length of suction nozzle and diffuser section was kept $L_s = L_d = 47mm$. Primary fluid (Air) was injected through motive convergent divergent nozzle with dimeters $d_1 = 20\ mm, d_2 = 9.50\ and\ d_3 = 10.66\ mm$ at inlet, throat and exit respectively. Throat dimeter of the jet pump is $d_{th} = 28\ mm$. Simulation were carried out by varying S/d_{th}(0.5-3), motive nozzle pressure(200kPa-800 kPa, and pressure head of water inlet reservoir (101kPa-102kPa). Here, S is the distance of the motive nozzle from the start of mixing chamber as shown in the Fig. 1. Set of the simulations conducted with different parameters are listed in the Table 1.

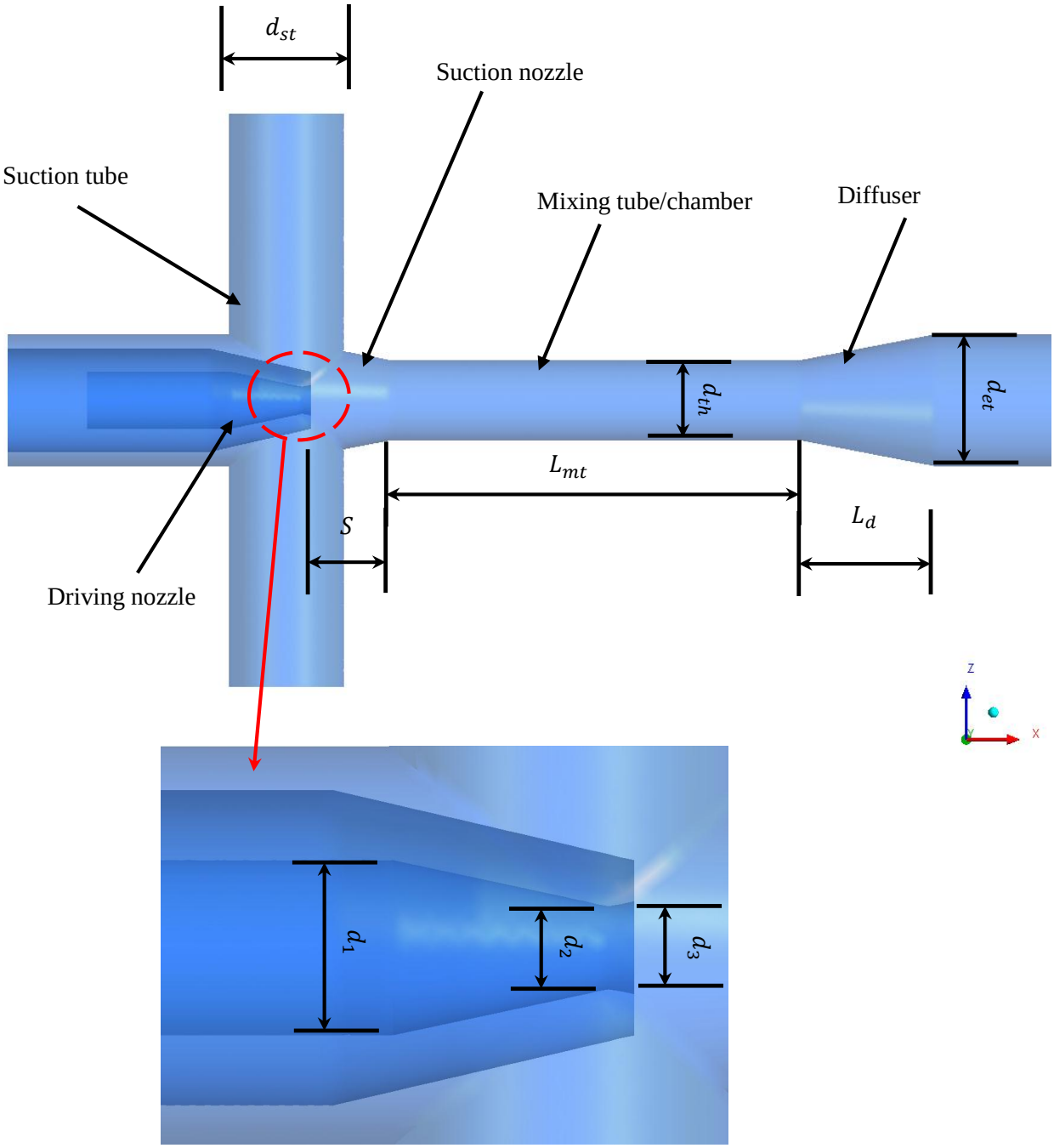

Figure 1: Geometrical details of the jet pump

Table 1: Summary of the simulations conducted

Simulation	p_m [k pa]	p_s [k pa]	S/d_{th}
A1-A7	200 , 250, 300, 350, 400, 450,500	101	0.5
B1-B7	200 , 250, 300, 350, 400, 450,500	102	0.5
C1-C7	200 , 250, 300, 350, 400, 450,500	103	0.5
D1-D-7	200 , 250, 300, 350, 400, 450,500	101	1.0
E1-E7	200 , 250, 300, 350, 400, 450,500	102	1.0
F1-F7	200 , 250, 300, 350, 400, 450,500	103	1.0
G1-G7	200 , 250, 300, 350, 400, 450,500	101	1.5
H1-H7	200 , 250, 300, 350, 400, 450,500	102	1.5
I1-I7	200 , 250, 300, 350, 400, 450,500	103	1.5
J1-J7	200 , 250, 300, 350, 400, 450,500	101	3
K1-K7	200 , 250, 300, 350, 400, 450,500	102	3
L1-L7	200 , 250, 300, 350, 400, 450,500	103	3

Mesh generation and boundary conditions

Total pressure boundary conditions was applied at the inlet section of the motive nozzle along with specifying the α_a = 1 and$\alpha_w = 0$. Thus, only air was allowed to enter from this boundary under different conditions of total pressure listed in the Table. 1. In the same manner, total pressure boundary condition was applied at secondary flow inlet for water by specifying α_a = 0 and$\alpha_w = 1$. At the outlet static pressure condition was applied. Location of outlet was placed far from the diffuser section to avoid presence of any gradients on it that can lead to unstable solution. Bounding surfaces of the flow were assigned with walls with no slip and adiabatic conditions. Locations of the above mentioned boundary conditions are shown in the Fig. 2.

Computation domain was discretized using ICEM CFD using hexahedral elements. As SST turbulent model is used as discussed above, thevalue of y-plus was maintained less than 2 at thewall to capture the boundary layer accurately. Additional 15 number of nodes were maintained within the boundary layer thickness. In order to achieve values of required y-plus and to restrict 15 nodes with in the boundary layer thickness, a procedure was adopted that is explained elsewhere in [14]. Computational mesh in the nozzle section is shown in the Fig. 3.

A mesh optimization study was carried out to get results independent of the mesh along with minimizing the computational time for the simulations. For mesh independence study total four meshes were generated i.e., A, B, C and D. Details about the node distribution is shown Fig. 4 and Table 2.A case with 200 kPa of primary air pressure and 10 cm pressure head in water side was computed using all four meshes. A comparison of computational time, memory allocated by the solver and computed ratio of water to air mass flow rate $(\frac{\dot{m}_w}{\dot{m}_a})$ has been presented in the Table 2. Results suggest that results obtained from Mesh C and D are almost same thus mesh C was selected for all other simulations due lesser memory requirements and computational time.

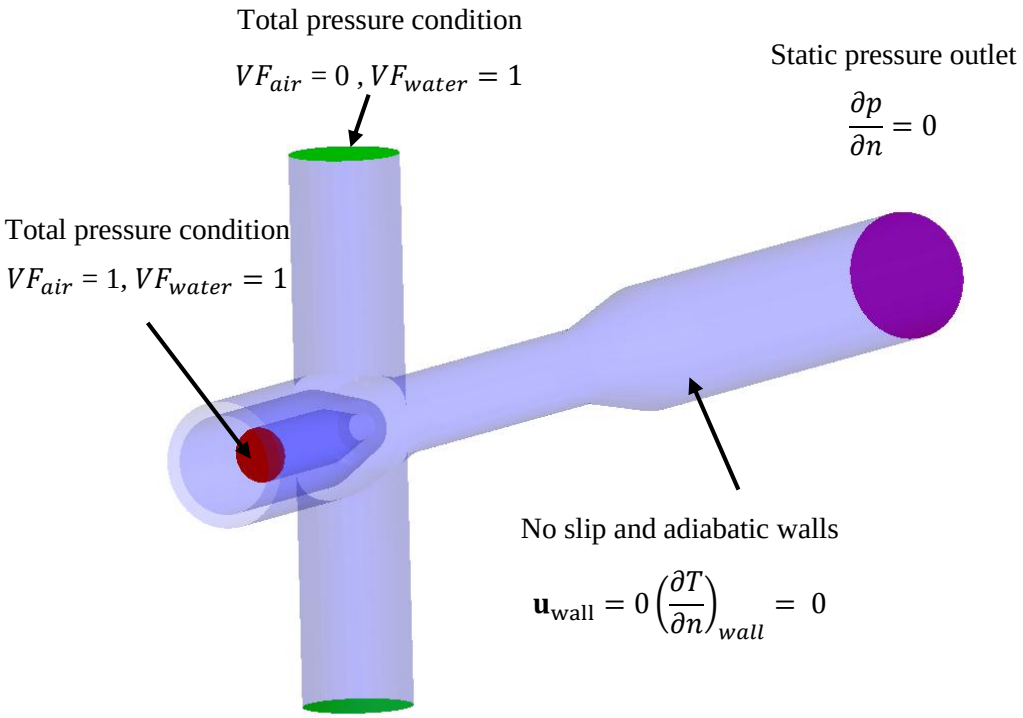

Figure 2: Details of the boundary conditions

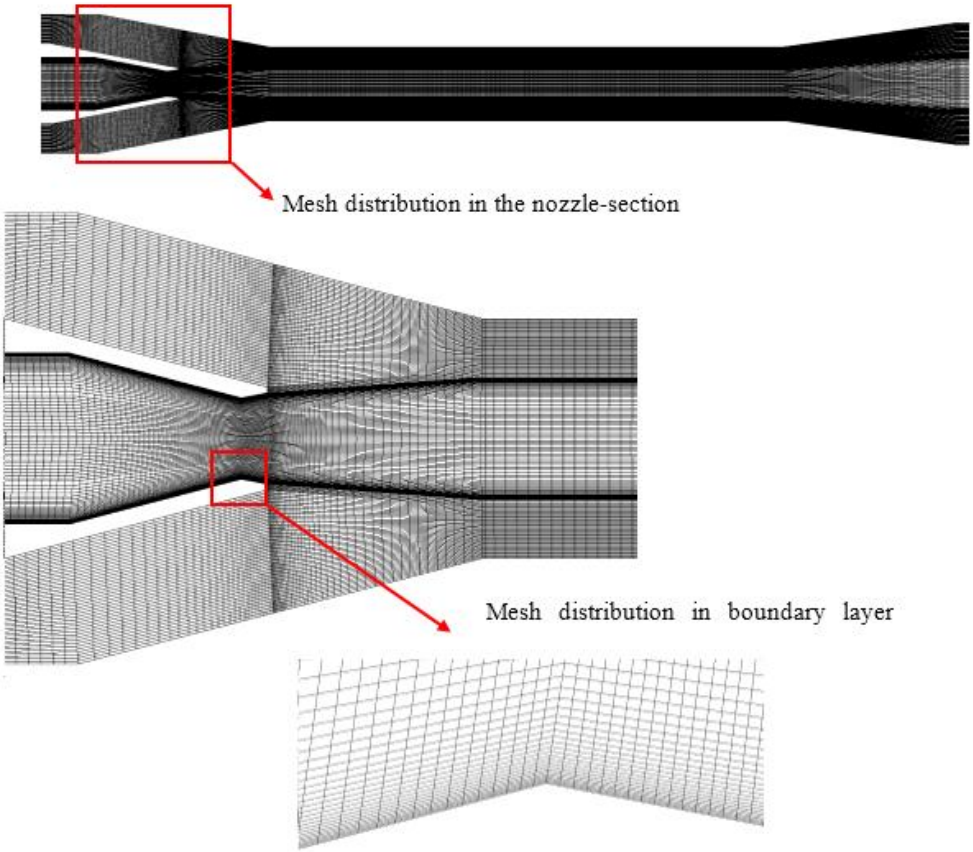

Figure 3: Mesh distribution in the nozzle section

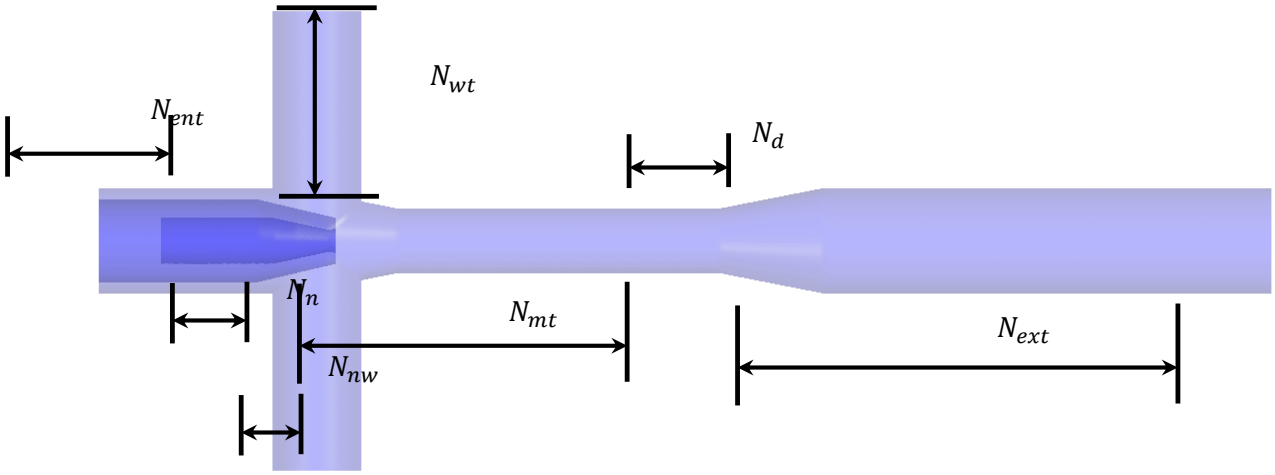

Figure 4: Node distribution on the jet pump geometry

Table 2: Mesh independence study

	Number of nodes in entry region(N_{ent})	Number of nodes in nozzle region(N_n)	Number of nodes in nozzle wake region(N_nw)	Number of nodes in mixing tube region(N_{mt})	Number of nodes in diffuser region(N_d)	Number of nodes in extended region(N_{ext})	Number of nodes in the water supply tube (N_{wt})	Number of nodes in circumferential direction(N_{cir})	Nodes in radial direction	Total mesh size [nodes]	Computational time for 10 iterations [s]	Computation memory required [Mb]	$\dot{m}_w/\dot{m}_a$
A	20	55	40	60	20	60	20	30	100	885000	645	12595.2	53.37
B	25	70	50	70	25	70	30	40	150	2220000	1008	18944	50.12
C	30	80	60	80	30	80	40	50	200	4400000	2245	30842.88	48.63
D	35	90	70	90	35	100	50	60	200	6240000	3814	41216	48.67

RESULTS

Figs. 5-8 shows variation of the mass flow rate of the secondary fluid with change of mass flow rate of primary fluid (air) for different values of suction head and S/D_{th}. Mass flow rate of secondary fluid increases linearly with the increase of primary fluid flow rate for all values of S/D_{th}. Flow rate of secondary fluid also increases with the increase of suction head. Flow rate of secondary fluid is more sensitive to suction head at higher flow rates of the primary fluid. It could be observed from Figs. 5-8 that gap between the lines widen up with the increase of flow rate of the primary fluid. On the other hand, value of mass flow of water does not increase monotonically with increase of ratio $\frac{S}{D_{th}} = 0.5$ to $\frac{S}{D_{th}} = 3.0$. Flow rate of secondary fluid flow rate increases with the increase of ratioS/D_{th} initially i.e. $\frac{S}{D_{th}} =$ 0.5 to $\frac{S}{D_{th}} = 3.0$, afterwards it decreases with increase of $\frac{S}{D_{th}} =$ 0.5 to $\frac{S}{D_{th}} = 3.0$. Maximum value of mass flow rate of secondary fluid was observed 7.93 kgs^{-1} that is corresponding the 0.08 kgs^{-1} flow rate of primary fluid for suction head of $H = 30\ cm$ and$\frac{S}{D_{th}} = 1.0$. While minimum value of secondary fluid mass flow rate was observed as 0.86 kgs^{-1} that is

corresponding the 0.02 kgs^{-1} flow rate of primary fluid for suction head of $H = 10\ cm$ and $\frac{S}{D_{th}} = 3.0$.

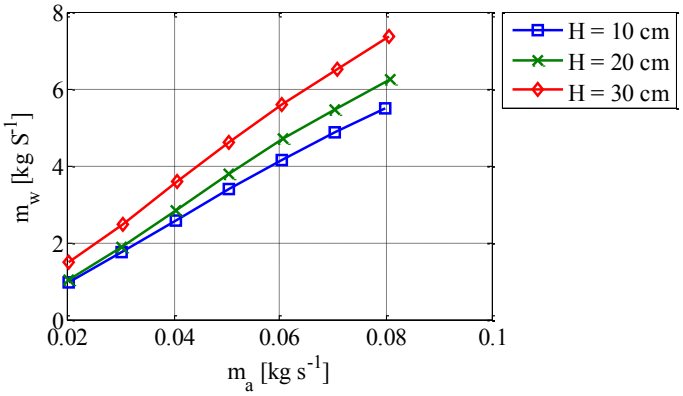

Figure 5: Variation of mass flow rate of secondary fluid (water) with primary fluid (air) at $\frac{S}{Dth} = 0.5$

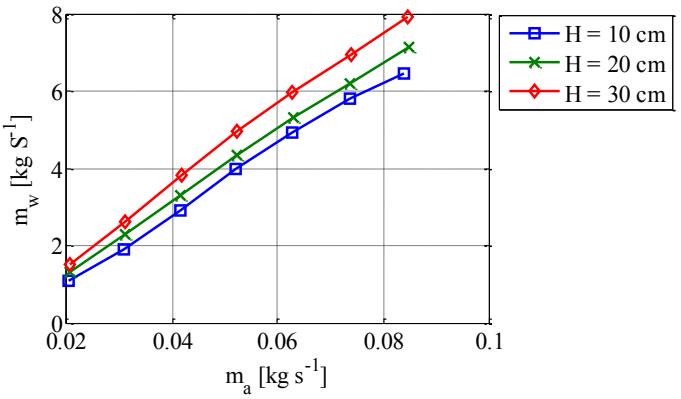

Figure 6: Variation of mass flow rate of secondary fluid (water) with primary fluid (air) at $\frac{S}{Dth} = 1.0$

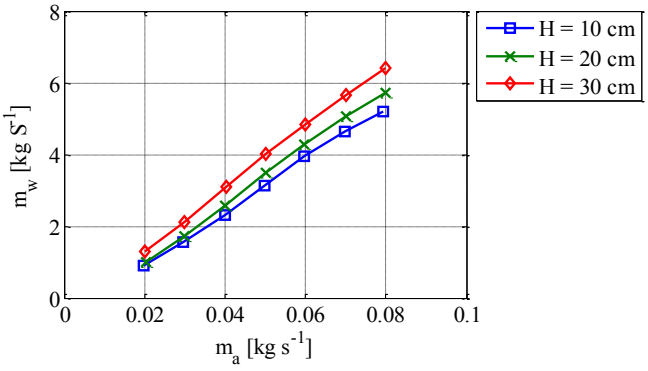

Figure 7: Variation of mass flow rate of secondary fluid (water) with primary fluid (air) at $\frac{S}{Dth} = 1.5$

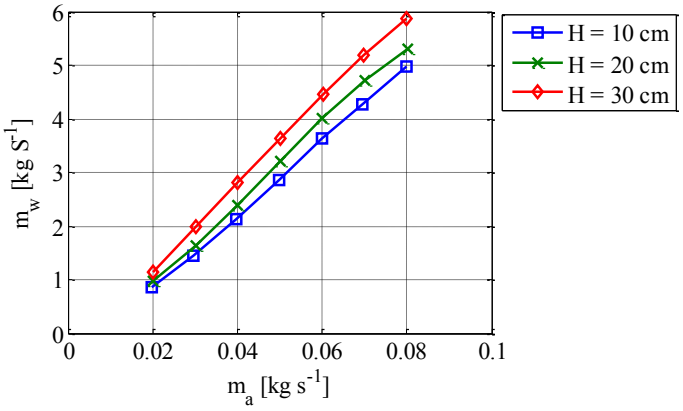

Figure 8: Variation of mass flow rate of secondary fluid (water) with primary fluid (air) at $\frac{S}{Dth} = 3.0$

Figs. 9-12 shows variation of $\frac{m_w}{m_a}$ with the primary fluid pressure for different values on suction head and $\frac{S}{D_{th}}$ ratio. Values of primary fluid pressure was changed from 200kPa to 250 kPa with an increment of 50kPa. It was observed that $\frac{m_w}{m_a}$ increases initially with the increase of primary fluid pressure and afterwards becomes constant or decrease slightly with further increase of P_a. Similar behavior was observed for all values of suction station head and $\frac{S}{D_{th}}$. In fact mass flow rate of the primary fluid through the nozzle is governed by primary fluid pressure P_a and back pressure P_b. Back pressure P_b was kept constant thus in this study so primary fluid flow rate just depend on the pressure with which the primary fluid is being injected in the pump. Primary fluid mass flow rate m_a increase with increase of p_a that indirectly increase in the flow rate of secondary fluid based on the greater energy transfer in the mixing chamber. As p_a in this only function of m_a thus its values is almost same for a particular value of Pa and different values of suction head (H) and the ratio $\frac{S}{D_{th}}$. Maximum value of $\frac{m_w}{m_a}$ was observed 94.83 that is corresponding the 400 kpa pressure of primary fluid for a suction head of $H = 30\ cm$ and $\frac{S}{D_{th}} = 1.0$. While minimum value of $\frac{m_w}{m_a}$ was observed as 47 that is corresponding the 200 kPa of primary fluid pressure at a suction head of $H = 10\ cm$ and $\frac{S}{D_{th}} = 3.0$. Moreover, it could be seen that percentage increase in the $\frac{m_w}{m_a}$ decreases with increases of suction head in all cases. For $\frac{S}{D_{th}} = 1.0$ and $p_a = 200kPa$, percentage increase in $\frac{m_w}{m_a}$ is noted 37% by increasing the suction head from 10cm to 30cm. This increase in the mass ratio $\frac{m_w}{m_a}$ reduces to 21% at higher value of primary fluid pressure i.e., at $p_a = 500\ kPa$.

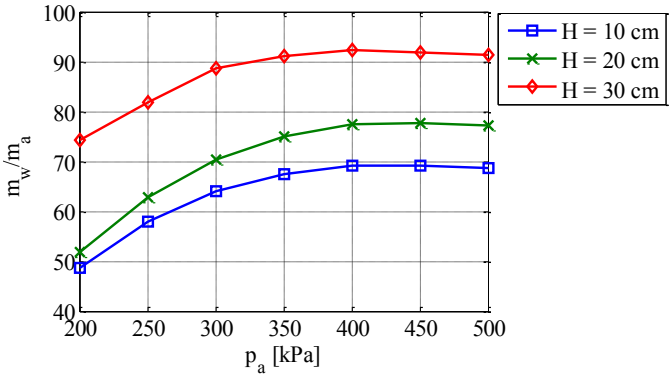

Figure 9: Variation of mass flow rate ratio of secondary fluid (water) to primary fluid (air) with pressure at $\frac{S}{Dth} = 0.5$

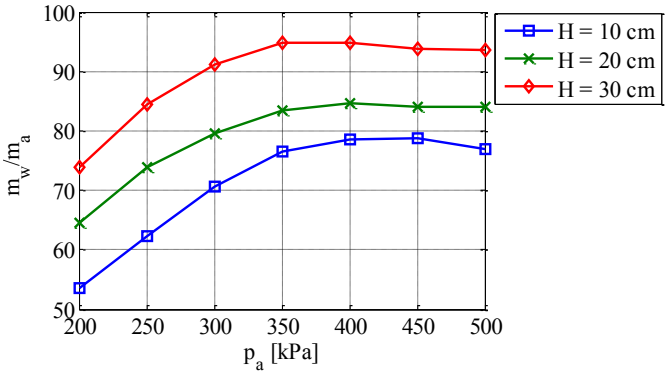

Figure 10: Variation of mass flow rate ratio of secondary fluid (water) to primary fluid (air) with pressure at $\frac{S}{Dth} = 1.0$

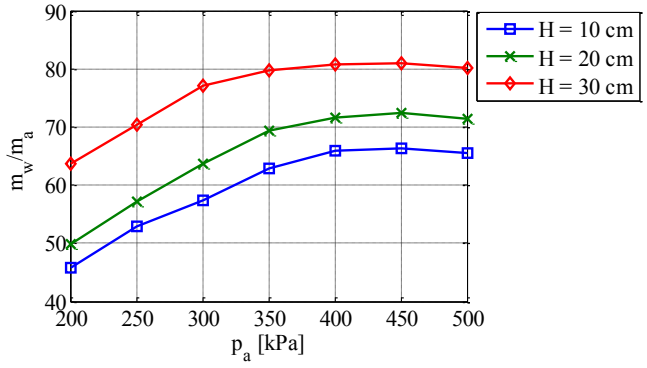

Figure 11: Variation of mass flow rate ratio of secondary fluid (water) to primary fluid (air) with pressure at $\frac{S}{Dth} = 1.5$

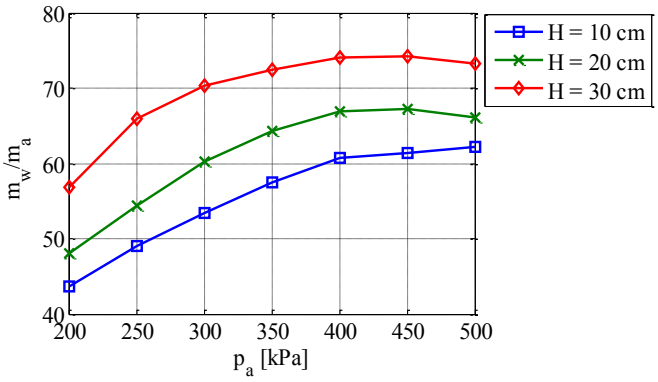

Figure 12: Variation of mass flow rate ratio of secondary fluid (water) to primary fluid (air) with pressure at $\frac{S}{Dth} = 3.0$

FLOW CHARACTERISTICS IN THE GAS-LIQUID EJECTOR

In the case of gas-liquid ejectors flow in the nozzle wake and mixing chamber is quite complex due compressible primary fluid flow through the convergent-divergent nozzle of ejectors. It effects the performance of ejectors to a great extent. Thus, it is mandatory to understand the flow physics in the mixing chamber for efficient design choices of thenozzle and mixing chamber for the gas-liquid ejectors. Getting Understanding of such phenomenon through flow visualization techniques experimentally could be too expensive and time-consuming. On the other hand, Computational Fluid Dynamics approaches in this regard could fulfill the purpose effectively with muchless effort and time. In the current study, CFD simulations have been conducted for various pressures of primary fluid p_a, suction pressure head (H) and ratio $\frac{S}{Dth}$. Fig. 13 shows the pressure and Mach no. distributions on the center line of jet ejectors for different values of primary fluid intake pressure (p_a). It could be seen that pressure and Mach no. values increases and decreases along the center line that shows the presence of shock waves in the wake of the nozzles. Presence of these shock waves could also be witnessed in the Figs. 14 &15 that shows Mach no. contour corresponding to different primary fluid pressures and pressure contours for a specific conditions respectively. It could be deducted from the Figs. 13-14 nozzle pressure at the exit is much less than the back pressureP_b. This situation implies that the nozzle is exhibiting over expended conditions for all the cases. Under these conditions flow undergoes compression and expansion repeatedly under virtual nozzles effects and these regions of compression and expansions could be clearly witnessed in Figs 13-15. These series of shock waves in the mixing tube is called shock train. This phenomenon comes with the conditions of over expended nozzle that is the case with all the simulations in this study. However, with the effect of the other conditions such under-expended and optimal conditions should be

evaluated that currently out of scope of this study.

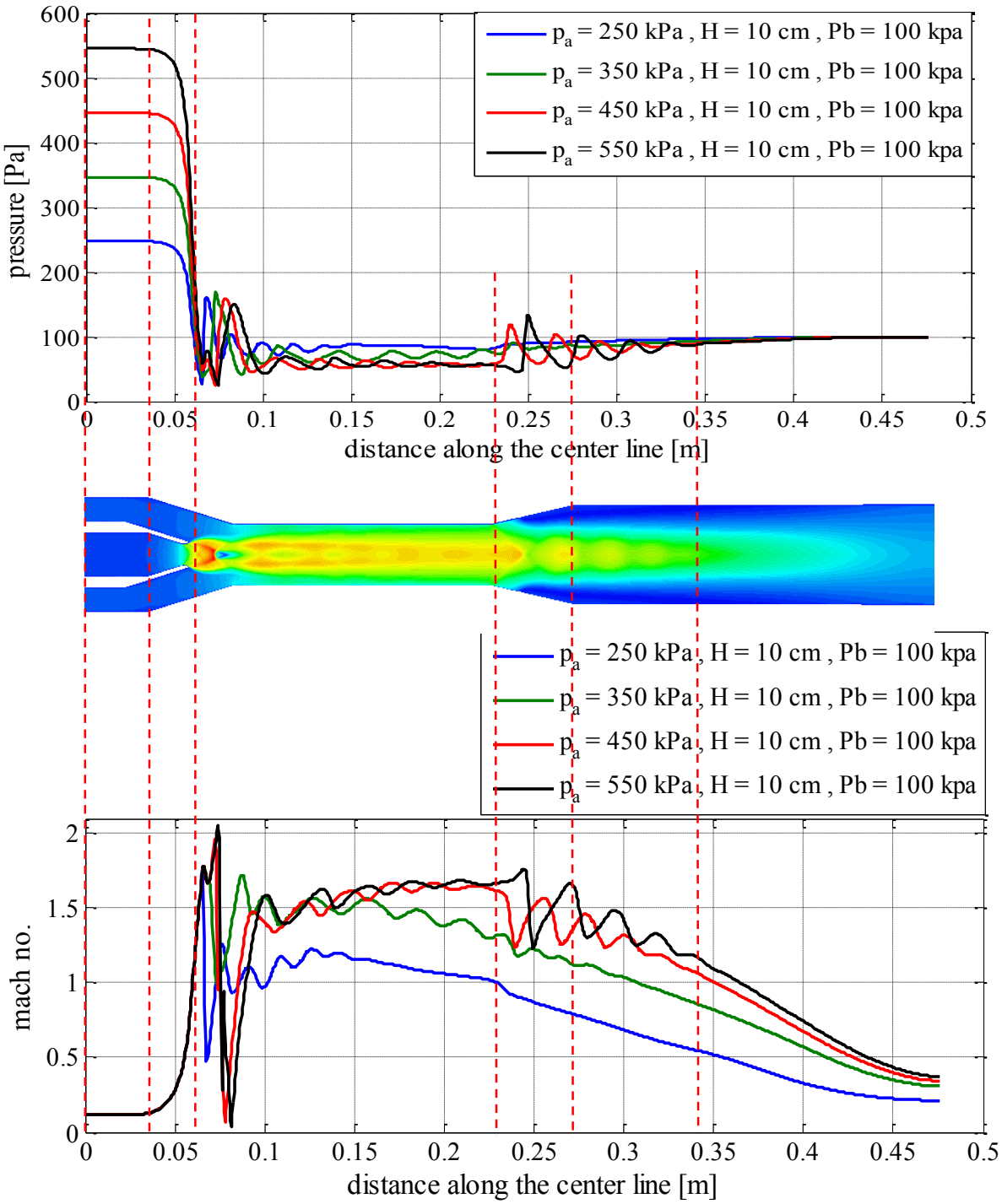

Figure 13: Pressure and Mach no. distribution along the length of the jet pump on the center line of the jet pump

As it could be seen in Fig. 13-15 pressure and Mach number fluctuates in the nozzle wake and mixing chamber as a result of multiple shock waves. During an expansion process when pressure decreases Mach number increases and vice versa. In the region of these shock waves when pressure and Mach number keep fluctuating, secondary fluid flow moves with its own velocity field that is on theslower side. This forms an intensive non-uniform velocity field that leads to a momentum exchange process in the mixing tube. This momentum transfer is based on the interphase drag forces and turbulent eddies. Fig.

16 shows contours of thevolume fraction of air where the region of momentum exchange process is shown on the central plane of the jet ejector. Figs. 13 & 14 shows that higher the primary fluid pressure at the inlet of nozzle p_a more it drops in the mixing chamber region and higher the Mach number is achieved by the primary fluid. Higher Mach number in the mixing tube ensures more momentum exchange that results in higher velocities and mass flow rate of the secondary jet. That is the reason higher values of p_a results in higher flow rates of secondary flow rate.

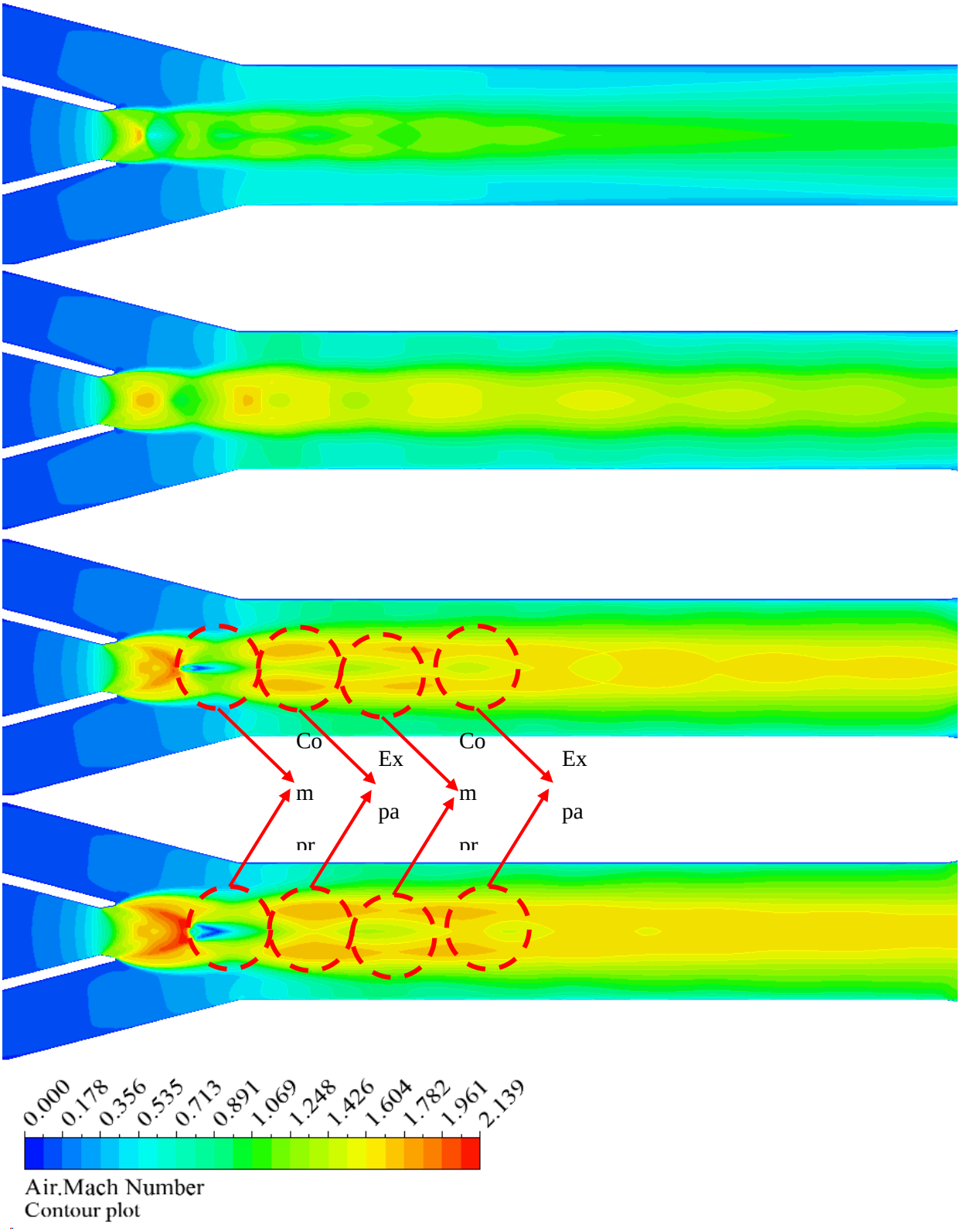

Figure 14: Mach no. distribution on the central plane for different primary fluid pressures

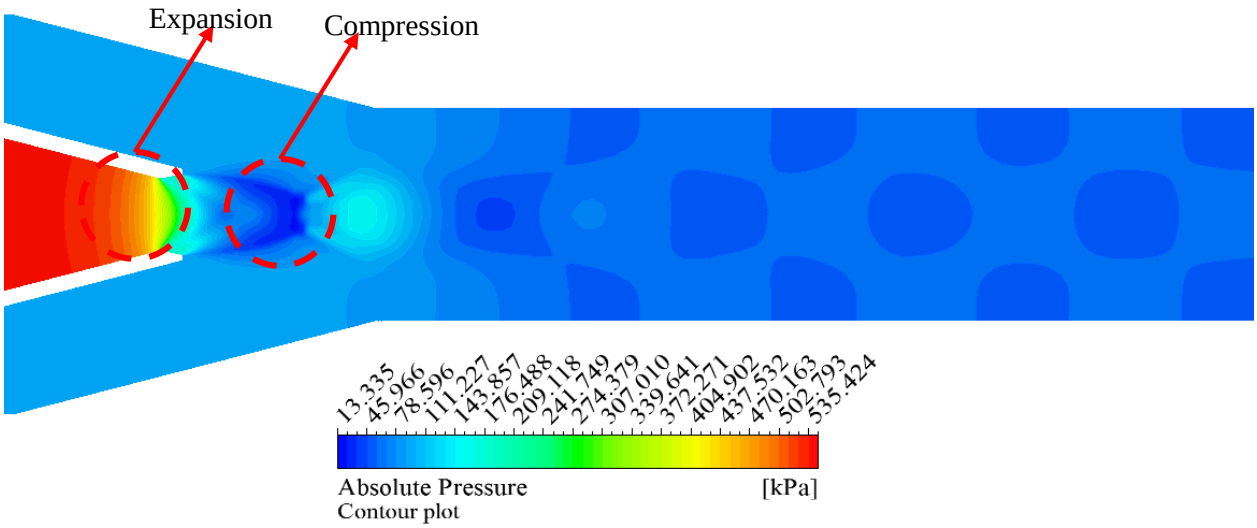

Figure 15: Pressure contours on the central plane

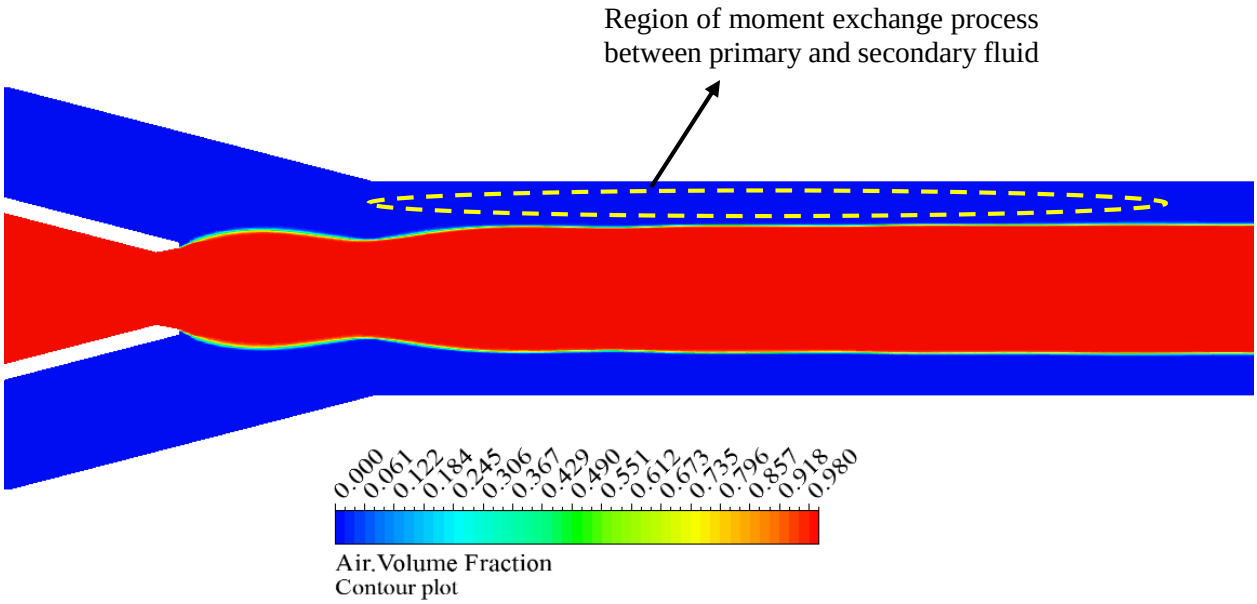

Figure 16: Air volume fractions contours on the central plan

CONCLUSIONS

Current study was conducted to understand the effect of primary fluid intake pressurep_a, suction pressure and $/D_{th}$. Moreover, flow characteristics in the nozzle wake and mixing tube are discussed using CFD techniques that are crucial in developing the flow behavior in the jet ejectors and will lead to a design of a better jet ejector system. Following observations were made from the current study.

- Flow rate of secondary fluid increases with the increase of p_a due to higher Mach value in the mixing tube correspond to higher values of p_a that enhances the momentum exchange process between the two phases.
- Mas ratio $\frac{m_w}{m_a}$ increases initially with increase of p_a and later on it stay constant for a while and then drop with the increase of p_a.
- Current simulations show the flow behavior in the nozzle wake and mixing chamber to explain the varying results with changing conditions. However, in

all cases nozzle was under over-expanded conditions. It is suggested behavior of the nozzle under under-expanded and optimum condition should also be studied for further understanding.

REFERENCES

[1] Y.N. Vasiliev, "Theory of a Two-Phase Gas-Liquid Ejector with Cylindrical Mixing Chamber," *Shoulder Mach. inkjet devices*, vol. 5, pp. 175–261, 1971.

[2] X. Song, M. Cao, W. Shin, W. Cao, S. Kang, and Y. Park, "Newcastle University ePrints Numerical Investigation of a Liquid-Gas Ejector Used for Shipping Ballast Water Treatment," 2014.

[3] a a Saker and H. Z. Hassan, "Study of the Different Factors That Influence Jet Pump Performance," vol. 2013, no. June, pp. 44–49, 2013.

[4] W. Liu and K. Pochiraju, "Back-Pressure Stall Prediction in Eductor-Jet Pumps," *46th AIAA Fluid Dyn. Conf.*, no. June, pp. 1–10, 2016.

[5] G. Cruz, E. L. Zaparoli, and C. R. De Andrade, "CFD ADJUSTED ONE-DIMENSIONAL JET PUMP MODEL N =," vol. di, 2007.

[6] E.Lisowski H.Momeni, "CFD modelling of a jet pump with circumferential nozzles for large flow rates," *F.Engineering*, vol. 10, no. 3, pp. 69–72, 2010.

[7] C. Li and Y. Z. Li, "Investigation of entrainment behavior and characteristics of gas–liquid ejectors based on CFD simulation," *Chem. Eng. Sci.*, vol. 66, pp. 405–416, 2010.

[8] H. Momeni, "Cdf Analysis of Water Jet Pump."

[9] G. Yuan, L. Zhang, H. Zhang, and Z. Wang, "Numerical and experimental investigation of performance of the liquid–gas and liquid jet pumps in desalination systems," *DES*, vol. 276, pp. 89–95, 2011.

[10] L. Grinis, N. Lubashevsky, and Y. Ostrovski, "Experimental and CFD Simulation of the Jet Pump for Air Bubbles Formation," vol. 10, no. 7, pp. 1234–1239, 2016.

[11] N. K. James Eves, Vassili V. Toropov, HarveyM. Thompson, "Fidelity Flow Analysis," no. September, pp. 1–8, 2010.

[12] R. Yapici and K. Aldas, "Optimization of water jet pumps using numerical simulation," *Proc. Inst. Mech. Eng. Part A J. Power Energy*, vol. 227, no. 4, pp. 438–449, 2013.

[13] F. R. Menter, "AIAA 93 · 2906 Zonal Two Equation k · co Turbulence Models for Aerodynamic Flows . Mailing Address : 24th Fluid Dynamics Conference FOR AERODYNAMIC FLOWS," 1993.

[14] M. Saeed, "Airborne wind turbine shell behavior prediction under various wind conditions using strongly coupled fluid structure interaction formulation," *Energy Convers. Manag.*, vol. 120, pp. 217–228, 2016.